Phase Separation and Multibody Effects in Three-Dimensional Active Brownian Particles

Francesco Turci* and Nigel B. Wilding
H. H. Wills Physics Laboratory, Tyndall Avenue, Bristol, BS8 1TL, United Kingdom

(Received 4 August 2020; accepted 14 December 2020; published 22 January 2021)

Simulation studies of the phase diagram of repulsive active Brownian particles in three dimensions reveal that the region of motility-induced phase separation between a high and low density phase is enclosed by a region of gas-crystal phase separation. Near-critical loci and structural crossovers can additionally be identified in analogy with simple fluids. Motivated by the striking similarity to the behavior of equilibrium fluids with short-ranged pairwise attractions, we show that a direct mapping to pair potentials in the dilute limit implies interactions that are insufficiently attractive to engender phase separation. Instead, this is driven by the emergence of multibody effects associated with particle caging that occurs at sufficiently high number density. We quantify these effects via information-theoretical measures of n-body effective interactions extracted from the configurational structure.

DOI: 10.1103/PhysRevLett.126.038002

Liquid-vapor phase separation and critical behavior are well-known characteristics of equilibrium fluids which stem from the presence of attractive interactions among their atoms or molecules [1,2]. Nonequilibrium many-particle systems can also display similar features: for example, assemblies of self-propelled (active) particles undergo—even in the absence of cohesive forces—a so-called motility-induced phase separation (MIPS) [3–5] between a high-density and low-density phase. Manifestations of this phenomenon in the form of aggregation have been observed both in suspensions of motile bacteria [6] and self-propelled colloids [7].

A key model that captures the essence of the physics of these systems is active Brownian particles (ABPs) [8], where the constituents interact via pairwise repulsive forces in the absence of hydrodynamic interactions [9]. Despite their nonequilibrium nature, some aspects of ABPs' behavior can be rationalized in terms of equilibrium concepts such as a pressure equation of state by incorporating out-of-equilibrium contributions and modifying equilibrium physical principles, e.g., by using an altered Maxwell construction [10–13].

A frequently highlighted feature of active systems is their "cooperativity," characterized in terms of the kinetics of the constituents and the pattern of their orientation in space [14,15]. Even for the simple case of ABPs, which lack an alignment mechanism, cooperative motion has been observed in two (2D) and three dimensions (3D) to give rise to complex patterns in the bulk and to engender phase separation [16,17]. Cooperative motion has also been suggested as a possible cause of the nonmonotonic response to the intensity of self propulsion—i.e., the activity—in the relaxation of active glasses [18].

Particle orientations are important to account for cooperatively and the microscopic explanation of collective effects in active matter [19]. However, to describe phase behavior, attempts have been made to construct minimal coarse-grained models that retain only particle coordinates or a continuum density profile, similar to simple models of equilibrium fluids [5,10,20–24]. Within this approach, the influence of orientational correlations is subsumed into "effective" interparticle interaction parameters.

In this Letter, we develop further the effective interaction approach to gain novel insight into phase separation and cooperativity. We first establish in detail the properties of a 3D system of ABPs including the phase diagram and critical point, together with features of the single phase region that also occur in equilibrium liquids namely a "Widom line" of maximum correlation length [25,26]; a line of maximum number density fluctuations; and a line of structural crossover—from exponential to oscillatory—known as the Fisher-Widom line [27,28]. We observe that the phase behavior is strongly reminiscent of that occurring in equilibrium fluids having a very short-ranged pair potential, with a critical point enclosed by the region of crystal-vapor phase separation and an order parameter broadly consistent with Ising universality. However, a coarse-grained model described by an effective pair potential derived in the low density limit is completely unable to account for MIPS. A quantitative analysis demonstrates, instead, that nonperturbative multibody interactions arise spontaneously in the active system, promoting effective attractions that ultimately drive the phase separation.

Previous simulation work has concentrated on 2D ABPs which display specific features such as an orientationally ordered hexatic phase [29,30]. The present study broadens the discussion to 3D ABPs where different phase behavior is expected [16,17]. In the model, particles interact via short-ranged, pairwise, repulsive interactions of the Weeks-Chandler-Anderson potential form with length-scale σ,

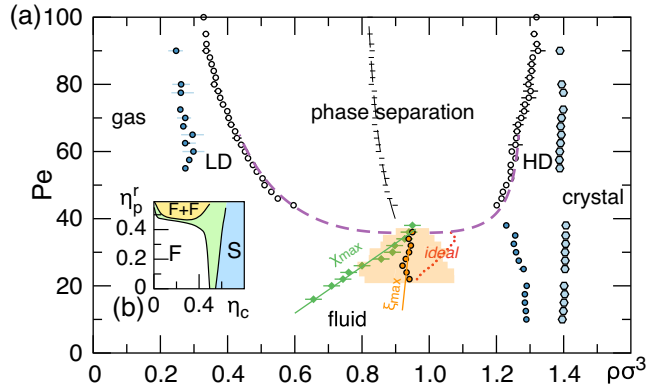

FIG. 1. (a) Phase diagram of 3D ABPs: empty circles correspond to the binodal of MIPS, separating a low density (LD) from a (HD) fluid; blue circles and hexagons are the fluid (or vapor) and crystal branches of fluid-solid coexistence; horizontal dashes are the coexistence diameter, fitted by a rectilinear diameter law $\frac{1}{2}(\rho_{\mathrm{LD}}+\rho_{\mathrm{HD}})=a\tau+\rho_c$. Lines of maximal ξ (orange), maximal $\chi/\chi_{\mathrm{ideal}}$ (green), crossover $\chi/\chi_{\mathrm{ideal}}=1$ (red dots) are also plotted. (b) Phase diagram of a colloid-polymer mixture with size ratio $q=0.4$ displaying fluid (F) solid (S) and metastable fluid-fluid coexistence ($F+F$) regions parametrized by the colloid and polymer reservoir packing fractions η_c, η_p, adapted from [31].

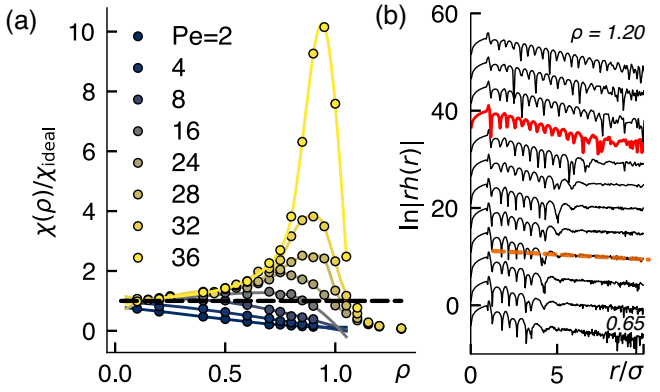

FIG. 2. (a) Estimates of $\chi/\chi_{\mathrm{ideal}}$ versus ρ. The horizontal dashed line marks the ideal gas value. (b) Total correlation function $h(r)$ for Pe = 28 measured for a selection of densities in [0.60, 1.20]. A dashed line (orange) shows a representative Ornstein-Zernicke fit to identify the bulk correlation length ξ. The red profile corresponds to density $\rho=1.05$, where $\chi/\chi_{\mathrm{ideal}}\approx 1$ and the exponential decay ceases.

have constant self-propulsion velocity v_0 and coupled translational and rotational diffusivities $D_t=D_r\sigma^2/3$, so that only the density ρ and the Péclet number $\mathrm{Pe}=v_0/(\sigma D_r)$ are the relevant control parameters. We first determine the phase diagram in the ρ-Pe plane. To do so, the system is initiated in an elongated, periodic simulation box (slab) with a pair of high-low density interfaces. We characterize the phases that emerge in the steady state. Previous work has focused on the MIPS between two disordered (fluidlike) phases, although studies in 3D also report the presence of an ordered face centred cubic crystal at high density and low Pe [17]. We confirm the stability of the crystalline phase at high Pe, and also trace lines of both crystal-vapor coexistence and a MIPS binodal to derive a complete phase diagram, Fig. 1(a).

The onset of MIPS is associated with critical behavior [16] and it is important to characterize the critical point and the near-critical region. In simple liquids exhibiting liquid-vapor (LV) criticality, the single phase region displays several crossover lines; in particular, lines of maxima of compressibility and correlation length are found which emanate from the critical point and serve as a means to estimate its location. We ask whether analogous features occur for a motility-induced critical point.

A block analysis [32,33] of the particle number fluctuations allows us to measure a quantity analogous to the relative compressibility of an equilibrium fluid $\chi/\chi_{\mathrm{ideal}}:=(\langle N^2\rangle-\langle N\rangle^2)/\langle N\rangle$, while the decay at large distances of the total correlation function $h(r)=g(r)-1$ allows us to determine the bulk correlation length ξ, see the Supplemental Material [34]. Figure 2(a) shows clearly that for $\mathrm{Pe}\gtrsim 10$ fluctuations grow with increasing Pe. The loci of the maxima of $\chi/\chi_{\mathrm{ideal}}$ and ξ identify two lines in the near-critical single phase region. Within numerical uncertainty, the crossing of the two lines provides a good estimate for the location of the critical point: $\rho_c\approx 0.94$ and $\mathrm{Pe}_c\approx 36$. In several equilibrium fluids [39] the supercritical density for which $\chi/\chi_{\mathrm{ideal}}=1$ closely approximates the so-called "Fisher-Widom" line of structural crossover, between a regime with oscillatory decay of the correlations to a regime with purely exponential decay, see Fig. 2(b). This line—Fig. 1(a)—is located at high densities and points to a structural crossover only close to the fluid-solid transition as discussed further in [34].

Since the Péclet number plays a role akin to the inverse temperature of equilibrium system, we follow a previous proposal [40] and define $\tau=|\mathrm{Pe}^{-1}-\mathrm{Pe}_c^{-1}|/\mathrm{Pe}_c^{-1}$ as the reduced Péclet number. We can then contrast several properties of MIPS with the behavior familiar from simple liquids. We find: (i) that the critical point is located at particular high densities, resulting in a rather asymmetric coexistence region (similarly to the 2D case [29,40]); (ii) that the near-critical region of the binodal can be fitted with Ising forms $\Delta\rho_i=A_i\tau^\beta$ with $\beta=\beta_{\mathrm{3D\,Ising}}=0.326$, consistent with recent on-lattice modeling of active particles [41]; (iii) while the coexistence diameter $d_\rho=(\rho_{\mathrm{LD}}+\rho_{\mathrm{HD}})/2$ does not vary linearly with respect to Pe, it does follow a linear relationship with respect to τ, $d_\rho=\rho_c+a\tau$, as in simple equilibrium liquids [42,43].

Our phase diagram shows that the MIPS region is enclosed within the region of crystal-vapor coexistence. Indeed, the overall topology of our phase diagram is reminiscent of that of equilibrium fluids having very short-ranged pair interactions [31,44]. Here, the archetypal system is a colloid (c)- polymer (p) mixture with size ratio $q=\sigma_p/\sigma_c$. q determines the range of effective

colloid-colloid interactions leading to colloid-rich and colloid-poor phase separation. When $q \ll 1$, the vapor-liquid binodal becomes metastable with respect to crystal-vapor coexistence. While in principle an effective one-component model requires a multibody description of the colloid-colloid interactions, in practice a short-ranged pair potential accurately accounts for the phase behavior for sufficiently small q [45,46].

Inspired by these similarities, we enquire whether it is possible to construct a coarse-grained effective equilibrium (or *passive*) model capable of reproducing the true phase behavior. An exact passive model will have interparticle interactions yielding the same probability of observing a given particle configuration as the active model. In general, one expects that this requires an effective Hamiltonian which is the sum of n-body contributions $H^{\mathrm{eff}} = \sum_{n=2}^{\infty} \theta_n$. Truncating this series at finite n yields an approximate passive model, e.g., $n = 2$ is the two-body approximation.

To gain systematic insight into the role of n-body effective interactions in the passive model, we study systems containing successively larger particle numbers $N = 2, 3, 4, \ldots$ in a box of volume V. The $N = 2$ system yields an exact effective pair potential $W_2(r)$ (see below). Studies of $N = 3$ ABPs provide information on three-body contributions to the effective interactions. Our method quantifies these not in terms of a three-body interaction potential θ_3 but in terms of the excess free energy of the *exact* effective passive model that describes $N = 3$ ABPs, compared to that of the approximate passive model of $N = 3$ particles interacting solely via the pair potential $W_2(r)$. In a similar way, a study of $N = 4$ particles yields information on the four-body contribution to the excess free energy unexplained by two- and three-body interactions.

Operationally, one computes the 1D probability distribution function $P_N(r_{\mathrm{min}})$ to find a minimal interparticle separation distance r_{min} among N ABP particles. Normalizing by the ideal gas probability yields $g'(r_{\mathrm{min}}) = P(r_{\mathrm{min}})/P^{\mathrm{ideal}}(r_{\mathrm{min}})$ whose asymptotic value at fixed volume $f_N = \lim_{r_{\mathrm{min}}\to\infty} g'(r_{\mathrm{min}})$ determines the ratio of the partition function of N particles to that of an ideal gas. The excess Helmholtz free energy of the exact effective passive system follows as $-k_B T \ln f_N = F_{\mathrm{ex}}$. The method can also be applied to measure F_{ex} for the approximate two-body system of N passive particles. The background to our method is described in detail in [47] and summarized in the Supplemental Material [34].

The effective pair interaction $W_2(r)$ for $N = 2$ ABPs is calculated for a given Pe as $W_2(r) = -\ln[g_2'(r)/f_2(V)]$, with $g_2'(r) = P_2(r_{\mathrm{min}})/P_2^{\mathrm{ideal}}(r_{\mathrm{min}})$ and $f_2 = \lim_{r_{\mathrm{min}}\to\infty} g_2'(r_{\mathrm{min}})$ [47]. The calculation is repeated for several values of Pe resulting in the forms shown in Fig. 3(a). This reveals that at low Pe the interaction is essentially repulsive and gradually develops an attractive well which becomes deeper as the Pe increases. We note that the range of the attraction is short compared to the size of the repulsive core,

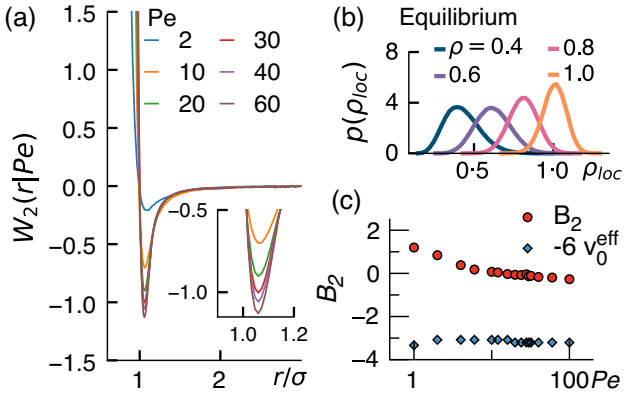

FIG. 3. (a) The effective pair potential $W_2(r|\mathrm{Pe})$ for several Pe. The inset magnifies the attractive region. (b) Distribution of local density for equilibrium simulations with pair interaction $W_2(r|\mathrm{Pe} = 60)$ and increasing ρ displaying a single phase. (c) Measured values of B_2 together with the criterion for phase separation.

in accordance with equilibrium models having a similar phase diagram topology, and that the shape of the potential is consistent with analytical approximations such as the unified colored noise approximation, known to reproduce the interactions in the weak activity regime [24].

Equipped with the forms of $W(r|\mathrm{Pe})$, we first enquire whether the attraction is sufficient to engender phase separation. Direct simulation with the potential $U(r|\mathrm{Pe}) = k_B T W_2(r|\mathrm{Pe})$ at $k_B T = 1$ demonstrates that this is not the case: for example, in Fig. 3(b) we show the distribution of local density around the particles for $\mathrm{Pe} = 60$ and several total densities well inside the phase separation region, see Fig. 1. The distributions are unimodal indicating that no phase separation occurs.

The failure of the effective pair potential to yield phase separation can be rationalized by analyzing the second virial coefficient $B_2 = -\frac{1}{2}\int (e^{-W_2(r)} - 1) d\boldsymbol{r}$ and comparing its trends with known criteria for phase separation in equilibrium systems. In simple liquids, the onset of LV phase separation occurs when $B_2 \approx -6 v_0^{\mathrm{eff}}$ where v_0^{eff} is the volume of an (effective) hard sphere [48,49]. This empirical criterion is particularly accurate in simple liquids with short-ranged attractions [50,51]. However, as shown in Fig. 3(c), B_2 for the effective pair potential for our ABP model never satisfies the criterion even at very large Pe. It follows that the effective, isotropic, two-body interactions obtained via coarse graining of the orientational degrees of freedom do not engender sufficiently strong effective attractions to induce phase separation. As shown in the Supplemental Material [34], the same conclusion holds in 2D.

While one might seek to correct this deficiency by reintroducing the orientational variables and describing the interactions via effective anisotropic short-ranged terms, we find that valuable insight can be gained by refining our calculations to include higher order

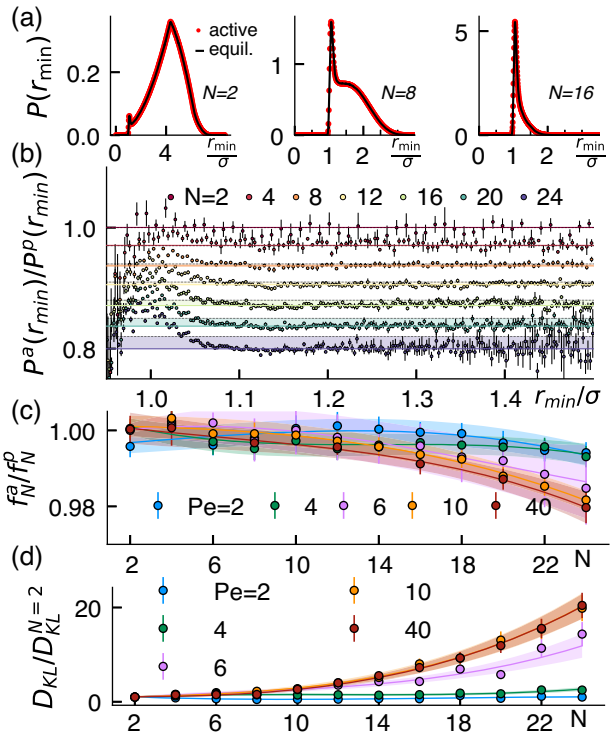

FIG. 4. (a) $P_N(r_{\min})$ for the active system (red circles) and the effective two-body passive system (black line) for three values of N at $\mathrm{Pe} = 40$. (b) Ratio $P_N^a(r_{\min})/P_N^p(r_{\min})$ at $\mathrm{Pe} = 40$ for increasing N. The shaded area indicates the growing gap between $P_N^a/P_N^p = 1$ and f_N^a/f_N^p: every curve is shifted vertically for clarity. (c) Ratio between the active and passive asymptotic contributions f_N as estimated from the limit of P_N^a/P_N^p. (d) Relative entropy D_{KL} between active and passive probabilities, scaled by the $N = 2$ value. Lines and shades in (c) and (d) are polynomial trends and confidence intervals, respectively.

contributions to the attraction, in the spirit of the multibody expansions of equilibrium systems [31]. To do so we compare the form of $P_N(r_{\min})$ for two systems: the active system at some prescribed Pe and an approximate passive system with the pair interaction $W_2(r|\mathrm{Pe})$. Specifically, we accumulate the PDFs $P_N^a(r_{\min})$ of the active and $P_N^p(r_{\min})$ of the passive case for N ranging from $N = 2$ to $N = 24$ in boxes of a fixed volume V, such that the number density ranges from $\rho = 0.003$ to $0.036\sigma^{-3}$. Comparing active and passive systems of such small N allows us to study systematically the effects of successively higher N-body interactions and demonstrate the emergence of collective contributions to the attraction that drives MIPS, similarly to the predictions of effective Fokker-Planck mappings [20].

Figure 4(a) shows that at first sight the passive probability distribution function closely reproduces the active ones at $\mathrm{Pe} = 40$. There are nevertheless subtle differences in the large $r_{\min}$ regime that grow with increasing Pe and which are key to understanding the origin of multibody effects. To expose these, we consider the ratio $P_N^a(r_{\min})/P_N^p(r_{\min})$ for various N. Results for $\mathrm{Pe} = 40$ are shown in Fig. 4(b) and reveal that on increasing N, the active particles are more likely than the passive ones to be found in close contact—a fact signaled by a relative depletion of the probability of finding a particle at large distances. The asymptotic value $\lim_{r\to\infty} P^a(r_{\min})/P^p(r_{\min}) = f_N^a/f_N^p$ is shown in Fig. 4(c) for a variety of choices of Pe. Its logarithm measures the free energy difference between the "exact" passive model of N ABPs and the approximate passive model described by $W(r)$. While at low Pe, f_N^a/f_N^p is close to unity for all the considered N, at sufficiently large $\mathrm{Pe} \gtrsim 6$, the ratio diminishes with increasing N. Remarkably, however, the deviation from unity becomes significant only for $N \gtrsim 12$, i.e., when the number of particles is close to the typical coordination number of a liquid. This suggests that a whole "cage" of active particles is needed to engender significant multibody attractions.

To quantify the difference between the prediction of the passive two-body model and the active system, we employ the so-called relative entropy, familiar from information theory, $D_{\mathrm{KL}}(P_N^a \| P_N^p) = \int_0^\infty P_N^a(r_{\min}) \log\left(P_N^a(r_{\min})/P_N^p(r_{\min})\right) dr_{\min}$. [52]. D_{KL} provides a scalar measure of the additional effects (or "surprisal") that the model P^p fails to capture [53]. In Fig. 4(d) we plot $D_{\mathrm{KL}}(N)/D_{\mathrm{KL}}(N = 2)$ for various Pe. At low activity, this ratio is independent of N: the two-body passive model provides an accurate representation of the active system. This remains true for Pe below about 6, whereafter the ratio gradually increases. The increase of D_{KL} is negligible for small N: three- or four-body terms do not contribute significantly to the enhanced attractions. Additionally, the behavior for $\mathrm{Pe} = 10$—which is just inside the range where enhanced near-critical fluctuations are discernible—is not markedly different from $\mathrm{Pe} = 40$. This implies an onset value of Péclet number that distinguishes a low activity regime (where multibody effects are negligible) and a high activity regime [12,54].

In conclusion, the phase behavior of 3D active Brownian particles exhibits striking similarities with that of simple liquids having very short-ranged attractions but it cannot be rationalized qualitatively in terms of effective two-body interactions. While the pair potentials that we derive in the low density limit are very short ranged, they fail to yield phase separation. We trace this fact to the need to include emergent multibody terms in the description of the effective model. While in many coarse-grained treatments of equilibrium systems the leading corrections to the pair potential description are given by three and four body interactions [46], for ABPs the principal multibody effect that boosts particle attraction and drives MIPS arises when particles become trapped in cages of coordination ≈12 or more [18,55]. Accordingly a mapping of active to equilibrium phase separation can only be achieved at the expense of the simplicity of the equilibrium model.

The authors thank R. Evans, T. Speck, and R. L. Jack for insightful conversations and critical reading of the manuscript. This work was carried out using the computational facilities of the Advanced Computing Research Centre, University of Bristol.

*Corresponding author.
f.turci@bristol.ac.uk

[1] B. Widom, Intermolecular forces and the nature of the liquid state: Liquids reflect in their bulk properties the attractions and repulsions of their constituent molecules, Science **157**, 375 (1967).
[2] J. V. Sengers and J. M. H. L. Sengers, Thermodynamic behavior of fluids near the critical point, Annu. Rev. Phys. Chem. **37**, 189 (1986).
[3] M. E. Cates and J. Tailleur, Motility-induced phase separation, Annu. Rev. Condens. Matter Phys. **6**, 219 (2015).
[4] M. C. Marchetti, Y. Fily, S. Henkes, A. Patch, and D. Yllanes, Minimal model of active colloids highlights the role of mechanical interactions in controlling the emergent behavior of active matter, Curr. Opin. Colloid Interface Sci. **21**, 34 (2016).
[5] A. P. Solon, J. Stenhammar, M. E. Cates, Y. Kafri, and J. Tailleur, Generalized thermodynamics of phase equilibria in scalar active matter, Phys. Rev. E **97**, 020602(R) (2018).
[6] G. Liu, A. Patch, F. Bahar, D. Yllanes, R. D. Welch, M. C. Marchetti, S. Thutupalli, and J. W. Shaevitz, Self-Driven Phase Transitions Drive Myxococcus Xanthus Fruiting Body Formation, Phys. Rev. Lett. **122**, 248102 (2019).
[7] I. Buttinoni, J. Bialké, F. Kümmel, H. Löwen, C. Bechinger, and T. Speck, Dynamical Clustering and Phase Separation in Suspensions of Self-Propelled Colloidal Particles, Phys. Rev. Lett. **110**, 238301 (2013).
[8] Y. Fily and M. C. Marchetti, Athermal Phase Separation of Self-Propelled Particles with No Alignment, Phys. Rev. Lett. **108**, 235702 (2012).
[9] M. C. Marchetti, J. F. Joanny, S. Ramaswamy, T. B. Liverpool, J. Prost, M. Rao, and R. A. Simha, Hydrodynamics of soft active matter, Rev. Mod. Phys. **85**, 1143 (2013).
[10] T. Speck, J. Bialké, A. M. Menzel, and H. Löwen, Effective Cahn-Hilliard Equation for the Phase Separation of Active Brownian Particles, Phys. Rev. Lett. **112**, 218304 (2014).
[11] R. G. Winkler, A. Wysocki, and G. Gompper, Virial pressure in systems of spherical active Brownian particles, Soft Matter **11**, 6680 (2015).
[12] E. Fodor, C. Nardini, M. E. Cates, J. Tailleur, P. Visco, and F. van Wijland, How Far from Equilibrium Is Active Matter, Phys. Rev. Lett. **117**, 038103 (2016).
[13] D. Levis, J. Codina, and I. Pagonabarraga, Active Brownian equation of state: Metastability and phase coexistence, Soft Matter **13**, 8113 (2017).
[14] C. Bechinger, R. Di Leonardo, H. Löwen, C. Reichhardt, G. Volpe, and G. Volpe, Active particles in complex and crowded environments, Rev. Mod. Phys. **88**, 045006 (2016).
[15] P. Pietzonka, É. Fodor, C. Lohrmann, M. E. Cates, and U. Seifert, Autonomous Engines Driven by Active Matter: Energetics and Design Principles, Phys. Rev. X **9**, 041032 (2019).
[16] J. Stenhammar, D. Marenduzzo, R. J. Allen, and M. E. Cates, Phase behaviour of active Brownian particles: The role of dimensionality, Soft Matter **10**, 1489 (2014).
[17] A. Wysocki, R. G. Winkler, and G. Gompper, Cooperative motion of active Brownian spheres in three-dimensional dense suspensions, Europhys. Lett. **105**, 48004 (2014).
[18] N. Klongvessa, F. Ginot, C. Ybert, C. Cottin-Bizonne, and M. Leocmach, Active Glass: Ergodicity Breaking Dramatically Affects Response to Self-Propulsion, Phys. Rev. Lett. **123**, 248004 (2019).
[19] T. Nemoto, E. Fodor, M. E. Cates, R. L. Jack, and J. Tailleur, Optimizing active work: Dynamical phase transitions, collective motion, and jamming, Phys. Rev. E **99**, 022605 (2019).
[20] T. F. F. Farage, P. Krinninger, and J. M. Brader, Effective interactions in active Brownian suspensions, Phys. Rev. E **91**, 042310 (2015).
[21] U. M. B. Marconi, M. Paoluzzi, and C. Maggi, Effective potential method for active particles, Mol. Phys. **114**, 2400 (2016).
[22] B. Trefz, S. Das, S. Egorov, P. Virnau, and K. Binder, Activity mediated phase separation: can we understand phase behavior of the nonequilibrium problem from an equilibrium approach, J. Chem. Phys. **144**, 144902 (2016).
[23] A. B. Slowman, M. R. Evans, and R. A. Blythe, Jamming and Attraction of Interacting Run-and-Tumble Random Walkers, Phys. Rev. Lett. **116**, 218101 (2016).
[24] R. Wittmann, U. M. B. Marconi, C. Maggi, and J. M. Brader, Effective equilibrium states in the colored-noise model for active matter ii. a unified framework for phase equilibria, structure and mechanical properties, J. Stat. Mech. 2017, 113208 (2017).
[25] L. Xu, P. Kumar, S. V. Buldyrev, S.-H. Chen, P. H. Poole, F. Sciortino, and H. E. Stanley, Relation between the Widom line and the dynamic crossover in systems with a liquid–liquid phase transition, Proc. Natl. Acad. Sci. U.S.A. **102**, 16558 (2005).
[26] J.-P. Hansen and I. R. McDonald, , *Theory of Simple Liquids: With Applications to Soft Matter* (Academic Press, New York, 2013).
[27] C. Vega, L. F. Rull, and S. Lago, Location of the Fisher-Widom line for systems interacting through short-ranged potentials, Phys. Rev. E **51**, 3146 (1995).
[28] A. Statt, R. Pinchaipat, F. Turci, R. Evans, and C. P. Royall, Direct observation in 3d of structural crossover in binary hard sphere mixtures, J. Chem. Phys. **144**, 144506 (2016).
[29] P. Digregorio, D. Levis, A. Suma, L. F. Cugliandolo, G. Gonnella, and I. Pagonabarraga, Full Phase Diagram of Active Brownian Disks: From Melting to Motility-Induced Phase Separation, Phys. Rev. Lett. **121**, 098003 (2018).
[30] J. U. Klamser, S. C. Kapfer, and W. Krauth, Thermodynamic phases in two-dimensional active matter, Nat. Commun. **9**, 5045 (2018).
[31] M. Dijkstra, J. M. Brader, and R. Evans, Phase behaviour and structure of model colloid-polymer mixtures, J. Phys. Condens. Matter **11**, 10079 (1999).

[32] M. Rovere, D. W. Hermann, and K. Binder, Block density distribution function analysis of two-dimensional Lennard-Jones fluids, Europhys. Lett. **6**, 585 (1988).
[33] D. Villamaina and E. Trizac, Thinking outside the box: Fluctuations and finite size effects, Eur. J. Phys. **35**, 035011 (2014).
[34] See Supplemental Material at http://link.aps.org/supplemental/10.1103/PhysRevLett.126.038002 for more details on the simulation model, a test for 2D ABPs of the Vligenhart-Lekkerkerker criterion, the analysis of correlations, finite-size effects, the multibody formalism with additional Refs. [35–38].
[35] S. Das, G. Gompper, and R. G. Winkler, Confined active Brownian particles: theoretical description of propulsion-induced accumulation, New J. Phys. **20**, 015001 (2018).
[36] S. Plimpton, Fast parallel algorithms for short-range molecular dynamics, J. Comput. Phys. **117**, 1 (1995).
[37] V. L. Kulinskii, The Vliegenthartt-Lekkerkerker relation: The case of the mie-fluids, J. Chem. Phys. **134**, 144111 (2011).
[38] Y. Liu, A. Z. Panagiotopoulos, and P. G. Debenedetti, Finite-size scaling study of the vapor-liquid critical properties of confined fluids: Crossover from three dimensions to two dimensions, J. Chem. Phys. **132**, 144107 (2010).
[39] D. Stopper, H. Hansen-Goos, R. Roth, and R. Evans, On the decay of the pair correlation function and the line of vanishing excess isothermal compressibility in simple fluids, J. Chem. Phys. **151**, 014501 (2019).
[40] J. T. Siebert, F. Dittrich, F. Schmid, K. Binder, T. Speck, and P. Virnau, Critical behavior of active Brownian particles, Phys. Rev. E **98**, 030601(R) (2018).
[41] B. Partridge and C. F. Lee, Critical Motility-Induced Phase Separation Belongs to the Ising Universality Class, Phys. Rev. Lett. **123**, 068002 (2019).
[42] A. Cornfeld and H. Carr, Experimental Evidence Concerning the Law of Rectilinear Diameter, Phys. Rev. Lett. **29**, 28 (1972).
[43] A. Z. Panagiotopoulos, Molecular simulation of phase coexistence: Finite-size effects and determination of critical parameters for two- and three-dimensional Lennard-Jones fluids, Int. J. Thermophys. **15**, 1057 (1994).
[44] M. Miller and D. Frenkel, Phase diagram of the adhesive hard sphere fluid, J. Chem. Phys. **121**, 535 (2004).
[45] K. Binder, P. Virnau, and A. Statt, Perspective: The Asakura Oosawa model: A colloid prototype for bulk and interfacial phase behavior, J. Chem. Phys. **141**, 140901 (2014).
[46] H. Kobayashi, P. B. Rohrbach, R. Scheichl, N. B. Wilding, and R. L. Jack, Correction of coarse-graining errors by a two-level method: Application to the Asakura-Oosawa model, J. Chem. Phys. **151**, 144108 (2019).
[47] D. J. Ashton and N. B. Wilding, Three-body interactions in complex fluids: Virial coefficients from simulation finite-size effects, J. Chem. Phys. **140**, 244118 (2014).
[48] G. Vliegenthart and H. N. Lekkerkerker, Predicting the gas–liquid critical point from the second virial coefficient, J. Chem. Phys. **112**, 5364 (2000).
[49] M. G. Noro and D. Frenkel, Extended corresponding-states behavior for particles with variable range attractions, J. Chem. Phys. **113**, 2941 (2000).
[50] J. Largo, M. Miller, and F. Sciortino, The vanishing limit of the square-well fluid: The adhesive hard-sphere model as a reference system, J. Chem. Phys. **128**, 134513 (2008).
[51] J. Largo and N. B. Wilding, Influence of polydispersity on the critical parameters of an effective-potential model for asymmetric hard-sphere mixtures, Phys. Rev. E **73**, 036115 (2006).
[52] S. Kullback and R. A. Leibler, On information and sufficiency, Ann. Math. Stat. **22**, 79 (1951).
[53] K. P. Burnham and D. R. Anderson, A Practical Information-Theoretic Approach, in *Model Selection and Multimodel Inference*, 2nd ed. (Springer, New York, 2002).
[54] M. Rein and T. Speck, Applicability of effective pair potentials for active Brownian particles, Eur. Phys. J. E **39**, 84 (2016).
[55] The identified multibody effects could be incorporated via a density dependent pair potential such as often arise in coarse-grained description of equilibrium systems. However, these are known for their inconsistencies [56].
[56] A. A. Louis, Beware of density dependent pair potentials, J. Phys. Condens. Matter **14**, 9187 (2002).